Controllable Self-Assembly of PbS Nanostars into Ordered Structures: Close-Packed Arrays and Patterned Arrays

Teng Huang, Qiang Zhao, Junyan Xiao, and Limin Qi*

Beijing National Laboratory for Molecular Sciences (BNLMS), State Key Laboratory for Structural Chemistry of Unstable and Stable Species, College of Chemistry, Peking University, Beijing 100871, People's Republic of China

ABSTRACT Controllable self-assembly of uniform star-shaped PbS nanocrystals with six symmetric ⟨100⟩-oriented horns into highly ordered structures including close-packed arrays and patterned arrays was realized by evaporation-induced assembly routes. First, large-area three-dimensional (3D) and two-dimensional (2D) hexagonal close-packed (hcp) arrays of PbS nanostars were assembled on clean Si substrate by drop coating and vertical deposition, respectively. Then, by using monolayer colloidal crystals (MCC) and inverted MCC (IMCC) as the template, a variety of non-close-packed (ncp) arrays of PbS nanostars with controllable patterns were fabricated through the vertical deposition method. With the MCC template, an ncp array of [111]-oriented PbS nanostars with three horns stably standing on the template plane was prepared, leading to the formation of novel star—sphere binary colloidal crystals with a stoichiometric star/sphere ratio of 1. The reflectance spectrum of the resultant MCC—PbS composite array was measured, which exhibited a considerable red shift in the reflectance peak compared with the original MCC template. Alternatively, with the IMCC template, an ncp array of [001]-oriented PbS nanostars with a single horn stretched vertically upward was obtained. Furthermore, some novel patterns for PbS ncp arrays were readily fabricated using MCC/IMCC templates with larger periodic spacings. For the template-assisted assembly of PbS nanostars, the obtained PbS ncp arrays generally inherited the long-range hexagonal order from the initial MCC template. This assembly strategy is a versatile approach and may open a new route for the controlled assembly of anisotropic nanostructured materials into large-scale ordered arrays with desirable patterns.

KEYWORDS: self-assembly · nanostars · patterning · ordered arrays · monolayer colloidal crystals

In recent years, organized assemblies of inorganic nanoparticles have attracted much interest because they can reveal fundamentally interesting collective physical properties and potential applications in functional devices.[1−3] Among numerous nanoparticle assembly strategies, evaporation-induced assembly could be the simplest method for fabricating both two-dimensional (2D) and three-dimensional (3D) assemblies, while Langmuir−Blodgett approach serves as an alternative technique for creating 2D assemblies effectively.[4,5] The self-assembly of nanoparticles into long-range ordered superlattices requires narrow size distribution and uniform shape of the particles. Therefore, the particle morphology is an important factor in governing the geometrical packing in organized structures.[6−9] It is noteworthy that, despite remarkable successes in the self-assembly of nearly monodisperse spherical colloidal nanoparticles,[10,11] the realization of controlled self-assembly of nonspherical nanocrystals is still challenging. Nowadays, researchers are paying more and more attention to anisotropic nanostructures because of the rich assembling behavior caused by their reduced shape symmetry and many peculiar properties owing to their unusual shape and/or mutual interaction.[12−14] For example, ordered mono- and multilayers in close-packed arrangement (2D and 3D assemblies) have been reported for anisotropic particle building blocks including nanorods,[15−18] ellipsoids,[19] nanoplates/nanosheets,[20−22] and faceted polyhedra.[15,23−25] Interestingly, binary superlattices self-assembled from triangular nanoplates and spherical nanoparticles have also been obtained.[10] Very recently, self-assembly of CdTe tetrapods into network monolayers has been realized at the air/water interface.[26] For preparing these 2D and 3D assemblies of nonspherical building blocks, either evaporation-induced assembly method[10,15−21,24] or Langmuir−Blodgett technique[22,23,25,26] is employed in most cases. However, to the best of our knowledge, the self-assembly behavior of well-defined star-shaped nanoparticles has not been reported yet.

Although evaporation-induced self-assembly has emerged as a conventional "bottom-up" method and receives much

*Address correspondence to liminqi@pku.edu.cn..

Received for review June 7, 2010 and accepted July 22, 2010.

Published online July 29, 2010. 10.1021/nn101272y

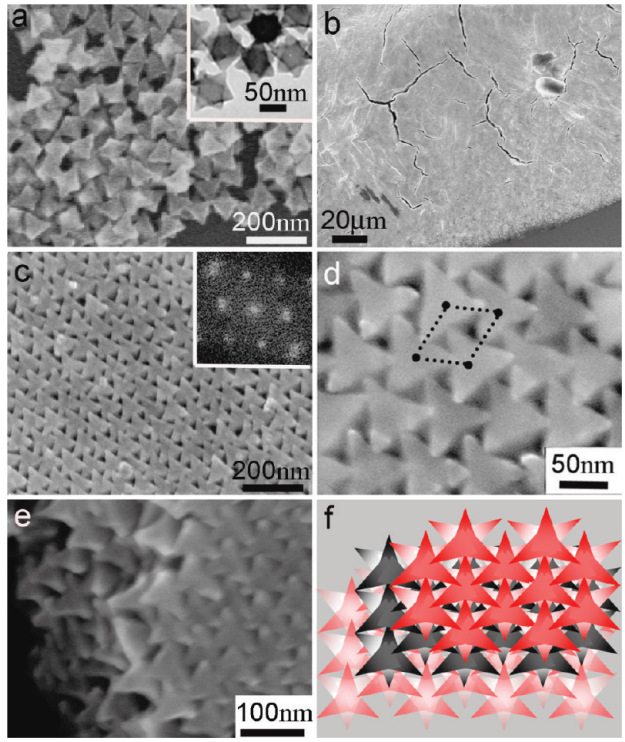

Figure 1. SEM images of (a) PbS nanostars and (b−e) their 3D hcp assemblies obtained by drop coating. (f) Schematic illustration of the 3D hcp structures of six-horn stars. Inset in (a) is the TEM image of PbS nanostars, and inset in (c) is the corresponding fast Fourier transform.

attention, generally only close-packed nanoparticle arrays form on normal substrates. It is still a main challenge to assemble nanoparticles in desired locations exhibiting controllable patterns. In this regard, template-assisted assembly, where a prefabricated "template" orients and directs the assembling components to control the morphology and pattern of the resulting assemblies, would provide a straightforward and effective route to fabricate novel structures/phases that would be otherwise unfavorable in the absence of the template.[3−5,27,28] A broad range of objects have been used as templates for nanoparticle organization, which can be classified into categories of soft and hard templates. While soft templates (such as small molecules and block copolymers,[29] as well as DNA molecules[30]) possess distinct chemical structures and provide multiple well-defined binding sites for the attachment of nanoparticles, such assembly strategies are typically applicable to a limited subset of particles that match specific surface chemistry requirements. Alternatively, hard templates, such as relief structures patterned on the surfaces of solid substrates,[31−33] provide greater toughness and preserve their structural characteristics for assembling nanoparticles. Nanosphere lithography that usually employs hexagonal close-packed (hcp) monolayer colloidal crystals (MCC) as the hard template has been proven to be a flexible and cost-effective technique for the patterning of nanostructured arrays with long-range periodicity in a large scale.[34−36] Recently, 2D periodic arrays of ring-shaped nanostructures assembled from CdSe semiconductor quantum dots were fabricated *via* an evaporative templating method by combining nanosphere lithography with capillary lithography.[37] However, little work has been focused on the periodic arrays of anisotropic nanoparticle building blocks with controlled patterns by the template-assisted assembly method.[38] Notable examples include the self-assembly of nanorods/nanotubes directed by the templates of polymers[39−42] and water droplets,[43] as well as the template-directed organization of CdTe nanotetrapods into lithographically patterned devices.[44] Considering the complex orientation and peculiar function for star-shaped nanoparticles, it would be highly desirable to assemble anisotropic nanostars with well-defined locations and orientations assisted by MCC.

Lead sulfide (PbS) is an important semiconductor with a narrow band gap (0.41 eV at room temperature) and large Bohr exciton radius (~18 nm), showing extensive quantum size effects in nanocrystalline form and great promise such as near-infrared (NIR) photoelectronic devices.[45,46] Although there has been great interest recently in self-assembly of PbS nanocrystals, the architectural control of PbS nanoscale building blocks with well-defined locations and orientations remains a key obstacle to overcome in the discovery of novel collective properties and is essential for the success of bottom-up approaches toward future nanodevices.[47−50] Herein, we report the evaporation-induced, controllable self-assembly of star-shaped PbS nanocrystals for the first time. First, large-area 3D and 2D hcp arrays of PbS nanostars were assembled on clean Si substrate by drop coating and vertical deposition, respectively. Then, a variety of non-close-packed (ncp) arrays of PbS nanostars with controllable patterns were fabricated on patterned Si substrate covered with MCC or inverted MCC (IMCC) using the vertical deposition method.

RESULTS AND DISCUSSION

Close-Packed Arrays of PbS Nanostars on Si Substrate. The synthesis of star-shaped PbS nanocrystals was achieved in the presence of the cationic surfactant cetyltrimethylammonium bromide (CTAB) and the anionic surfactant sodium dodecyl sulfate (SDS), as described in our previous work.[51] The PbS product exhibits a well-defined star-shaped geometry with six symmetrical horns oriented along the ⟨100⟩ directions, and the crystal size determined from the distance between two neighboring vertices is ~75 nm (Figure 1a and Supporting Information, Figure S1). The preparation process for 3D hcp assemblies of PbS nanostars is illustrated in Scheme 1A using the drop coating method. When one drop (~30 μL) of a concentrated PbS dispersion (~30 mM) was cast onto a Si substrate and dried in air, PbS nanoparticles spontaneously adopted ordered structures and precipitated to the substrate at the edge with slow solvent evaporation, which typically resulted in

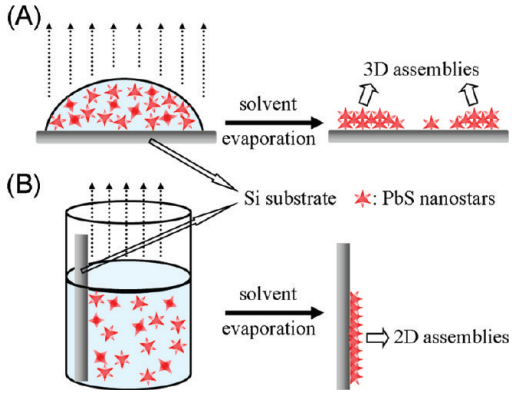

Scheme 1. Schematic illustration of two methods of evaporation-induced assembly: (A) drop coating, (B) vertical deposition.

formation of rings >100 μm in width due to the coffee-cup effect[52−54] (Supporting Information, Figure S2). Figure 1b shows that PbS nanostars self-assembled into films at the edge with a significant amount of cracks after solvent evaporation. Figure 1c shows an enlarged scanning electron microscopy (SEM) image of the obtained PbS assemblies, which suggests that the close-packed arrays exhibit hexagonal geometry in a large area, as indicated by the fast Fourier transform. As clearly shown in Figure 1d, PbS nanostars self-assembled into hcp arrays with an average distance between the centers of neighboring PbS particles of ~60 nm. Considering the peculiar morphology of six-horn stars, PbS nanoparticles tended to deposit with three horns stably standing on the lower layer or the substrate, and the horns of neighboring nanostars interdigitated to form assemblies with closest packing. An oblique view presented in Figure 1e confirms the multilayer 3D array of PbS nanostars. As expected from the hexagonal arrangement, each PbS monolayer is shifted by half the inter-PbS distance with respect to the adjacent layers (Figure 1f).

A simplified geometrical model was adopted to schematically illustrate the lattice spacing of 3D hcp nanostar assemblies (Scheme 2). It shows that the horns of neighboring six-horn nanostars interdigitate to form 3D hcp assemblies with closest packing. For such a closest packing, the center-to-center distance between two neighboring nanostars (d) should meet the equation $d = (\sqrt{3}/2)l - a$, where l represents the distance between two neighboring vertices of an individual nanostar and a represents the inserted distance between neighboring nanostars. For the current 3D hcp assemblies of PbS nanostars (as shown in Figure 1), l and d were measured to be ~75 and ~60 nm, respectively. It indicates that the inserted distance between neighboring nanostars (a) is around 5 nm, which is consistent with the experimental observation.

The vertical deposition is an effective method for the preparation of MCC with a 2D hcp structure, which was currently used to prepare 2D hcp assemblies of PbS

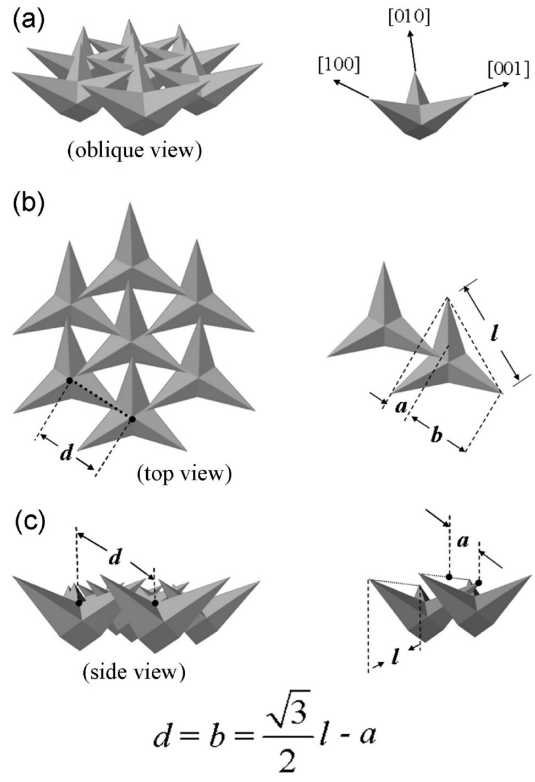

$$d = b = \frac{\sqrt{3}}{2} l - a$$

Scheme 2. Schematic illustration of the close-packed microstructure of 3D hcp nanostar assemblies showing the lattice spacing: (a) oblique view, (b) top view, (c) side view. For clarity, only one layer of half nanostars showing three upper horns is illustrated. Here, *d* represents the center-to-center distance between two neighboring nanostars. For the superficial plane formed by three upper vertices of each nanostar, *l* represents the distance between two neighboring vertices of an individual nanostar, *a* represents the inserted distance between neighboring nanostars, and *b* represents the vertex-to-vertex distance between two neighboring nanostars, which equals *d*.

nanostars. As illustrated in Scheme 1B, the assembly process here was carried out in a cuvette containing the aqueous dispersion of PbS nanostars with a vertically inserted Si substrate. At a proper concentration of the initial PbS dispersions (*e.g.*, ~1 mM), the monolayer 2D arrays of PbS nanostars could be fabricated after evaporating the dispersion medium. Figure 2 shows the SEM images of the obtained 2D assemblies of PbS nanostars. The nanostars self-assembled into monolayer hcp arrays very similar to the top layer arrangement of the 3D hcp assemblies. However, as shown in

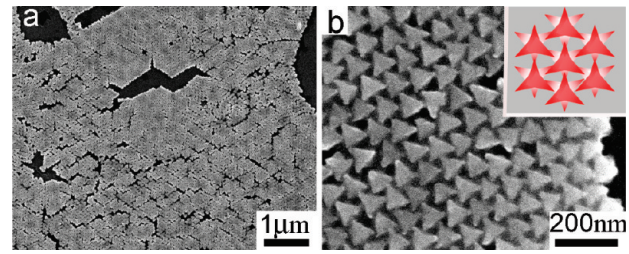

Figure 2. SEM images of 2D hcp assemblies of PbS nanostars obtained by vertical deposition. Color inset in (b) illustrates the 2D hcp structures of six-horn stars.

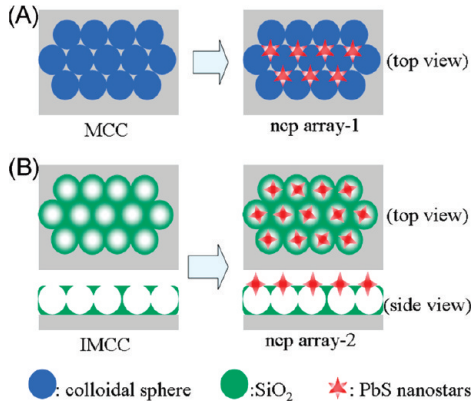

Scheme 3. Schematic illustration of the fabrication of ncp arrays of PbS nanostars assisted by MCC (A) and IMCC (B) through vertical deposition.

Figure 2b, the average spacing between two neighboring nanostars is ~70 nm, which resulted in a considerable deviation of orientation of nanostars for the 2D hcp arrays. It has been shown that high-quality colloidal crystals of monodisperse polymer or SiO_2 spheres can be readily prepared using the vertical deposition method.[55] For the preparation of MCC, colloidal crystallization is initiated by attractive capillary forces in the meniscus region, and solvent evaporation causes a convective particle flow toward the substrate from the bulk of colloidal suspension, so the balance between capillary forces and convective flow during the solvent evaporation is essential for the monotonic formation of MCC.[56] However, this simple approach is generally limited to colloidal particles that sediment slower than the solvent evaporation since the larger or denser particles tend to sediment quickly and are not deposited well.[57,58] Considering the relatively high density of the current PbS nanostars, the vertical sedimentation of PbS nanostars in the solution would be competitive with their deposition onto the vertical Si substrate.

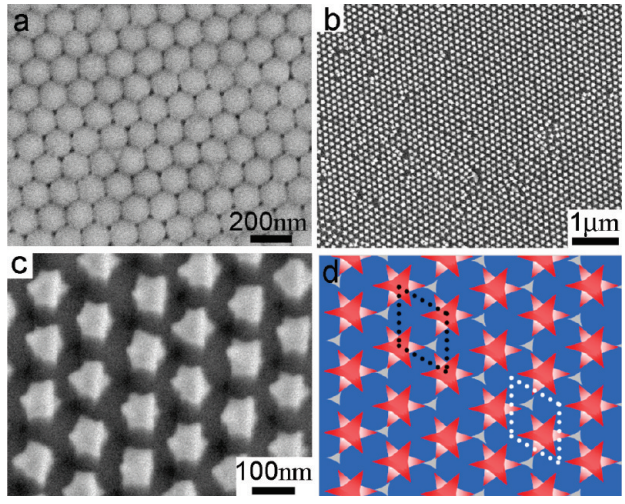

Figure 3. SEM images of (a) 130 nm MCC template and (b,c) 2D ncp array of PbS nanostars assembled on the template by vertical deposition. (d) Schematic illustration of the 2D ncp array-1 of six-horn stars.

Therefore, a considerable orientational deviation could occur due to the perturbation of particle sedimentation during the slow solvent evaporation.

Because the nanoparticles were passivated by surfactants, assembly could be dominated by repulsive electrostatic/steric interactions that favored close-packed structures. Here the surfactant concentration in the PbS dispersions should be high enough to make the particle positively charged and stable in water, which was critical for the formation of the 3D and 2D hcp assemblies. If the as-prepared nanocrystals were washed several times with deionized water, PbS nanostars with insufficient surfactant coating tended to aggregate in a disordered manner due to the large van der Waals attraction. Besides the surfactant concentration, the temperature for the solvent evaporation was also important for the preparation of 3D and 2D hcp assemblies of PbS nanostars. When the temperature was higher than 60 °C, only disordered PbS aggregates formed because the solvent evaporation was too fast for the PbS nanostars to attain their equilibrium positions.

Patterned Arrays of PbS Nanostars Assisted by MCC. Two kinds of patterned templates on Si substrates, which are denoted as MCC and IMCC, were used for the self-assembly of PbS nanostars into patterned arrays, as illustrated in Scheme 3. For the preparation of the ncp array of PbS nanostars with three horns stably standing on the template (designated as ncp array-1, Scheme 3A), the MCC template is employed to direct the vertical deposition. Considering that the PbS six-horn star is actually a single crystal with the six horns grown along the ⟨100⟩ directions[51] and it uses three ⟨100⟩-oriented horns to stand on the template, ncp array-1 can be regarded as [111]-oriented assemblies; namely, the [111] axis of the crystal is perpendicular to the plane of the template. Alternatively, patterned assemblies of [001]-oriented PbS nanostars with a single horn vertically standing on the template plane (designated as ncp array-2) can be fabricated using the IMCC template by vertical deposition, which is presented in Scheme 3B. It is worth mentioning that ncp arrays of PbS nanostars with both [111] and [001] orientations inherit the long-range hexagonal order from the initial MCC template.

Figure 3a shows the MCC template, in which the poly(styrene methyl methacrylate) (P(St-MMA)) spheres had an average diameter (*D*) of 130 nm and arranged hexagonally on the Si substrate in a large area. After vertical deposition of PbS nanostars on the MCC template, as shown in Figure 3b, a uniform film of PbS assemblies could deposit on the substrate. From a magnified image shown in Figure 3c, we can see that the voids among the neighboring P(St-MMA) spheres are the most stable positions for the deposition of PbS nanostars with three horns standing, and the spacing between two neighboring nanostars is 130 nm, as precisely predefined by the MCC template. Figure 3d illustrates the 2D ncp array-1 of PbS nanostars with the

[111] direction perpendicular to the template plane, which reserved the long-range hexagonal periodicity of the MCC template. It is worth noting that the resultant PbS arrays were also well-aligned with uniform side orientations. At a proper concentration of initial PbS dispersions (~1 mM), when one nanostar settled on one void, its stretched sharp tips prevented the deposition of other stars in the three neighboring voids. Thus, the PbS nanostars tended to occupy three separated interstitial sites in the ordered MCC template layer, which resulted in the ncp array-1 structure with the star-to-sphere number ratio of 1 (Figure 3d).

At a higher concentration of the initial PbS dispersion (~2 mM), as shown in Figure 4, more PbS nanostars can be trapped in the voids among the P(St-MMA) spheres after vertical deposition, resulting in a PbS nanostar array with a higher packing density, and the star-to-sphere number ratio is greater than 1 but less than 2. In this higher PbS dispersion concentration, when one nanostar settled on one void, other nanostars could also occupy some neighboring voids besides the three separated interstitial sites in the MCC template layer. However, when nanostars filled neighboring gaps, perfect structural order was not obtained due to the steric hindrance of PbS six-horn stars with stretched sharp tips. It may be noted that binary colloidal crystals consisting of one layer of larger spheres (L) and one layer of smaller spheres (S) with different stoichiometries (such as LS and LS_2) can be obtained *via* layer-by-layer assembly.[59] In the current situation, novel star−sphere binary colloidal crystals consisting of one layer of six-horn PbS nanostars and one layer of polymer spheres with a stoichiometric star/sphere ratio of 1 were obtained by assembly of PbS nanostars (l ~ 75 nm) onto MCC of polymer spheres (D ~ 130 nm) at a proper concentration of initial PbS dispersions (~1 mM). However, regular star−sphere binary colloidal crystals with a higher stoichiometric star/sphere ratio cannot be obtained at the fixed sizes of stars and spheres due to steric hindrance. Since the PbS nanostars with a double-tripod shape are potentially nestling into the triangle-shaped interstices among colloidal spheres, the optimum sphere size for the formation of star−sphere binary colloidal crystals with different stoichiometries can be calculated through a geometrical model shown in Scheme 4. It can be seen that there is a critical diameter (D_c) of colloidal spheres for the formation of star−sphere binary colloidal crystals with a star/sphere ratio of 2, which is equal to 2l. If the sphere diameter is smaller than D_c, star−sphere binary colloidal crystals with a star/sphere ratio of 1 can be obtained, but the formation of perfect binary colloidal crystals with a star/sphere ratio of 2 is prohibited since the stretched star tips would prevent the deposition of other stars in the three neighboring voids. When the sphere diameter is increased up to larger than D_c, star−sphere binary colloidal crystals with a star/sphere ratio of 2 can be obtained. Particularly, for the PbS nanostars with l ~ 75 nm, D_c would be ~150 nm; therefore, star−sphere binary colloidal crystals with a star/sphere ratio of 1 (*i.e.*, the ncp array-1 structure shown in Figure 3) were readily obtained using polymer spheres with a diameter slightly less than D_c (*e.g.*, ~130 nm). It may be expected that star−sphere binary colloidal crystals with a star/sphere ratio of 2 could be produced by selecting colloidal spheres with a diameter larger than 150 nm under suitable assembly conditions.

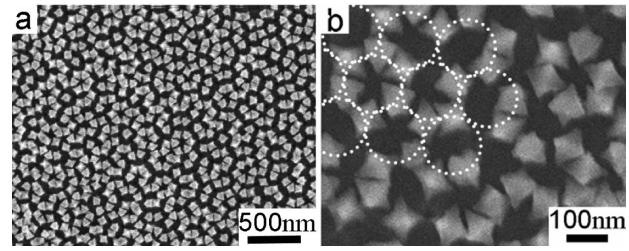

Figure 4. SEM images of PbS nanostar array assembled on the 130 nm MCC template with a higher packing density by vertical deposition. Circled areas in (b) represent the positions of colloidal spheres.

As a result of a 2D periodic change of refractive index for the ordered arrays of PbS nanostars assembled on the 130 nm MCC template, the as-obtained MCC−PbS composite arrays may demonstrate typical properties of photonic crystals. Here the photonic properties of the MCC−PbS composite arrays were preliminarily investigated by measuring their optical reflection spectra. With normal incidence, the reflection spectra of both composite arrays with different packing densities as well as the 130 nm MCC template showed obvious reflection peaks (Figure 5). This phenomenon has also been observed in the case of 2D ncp colloidal crystals.[60,61] As shown in Figure 5a, the reflection spectrum of the 130 nm MCC template showed a main peak centered around 330 nm. For the typical structure of composite arrays shown in Figure 3b−d with the star-to-sphere number ratio of 1 (designated as MCC-PbS-1), the refection spectrum exhibited a major maximum centered at 545 nm (Figure 5b). For another composite array with a higher packing density of PbS nanostars, as shown in Figure 4 (designated as MCC-PbS-2), the position of the main reflection peak further red-shifted to 690 nm (Figure 5c). Notably, after vertical deposition of

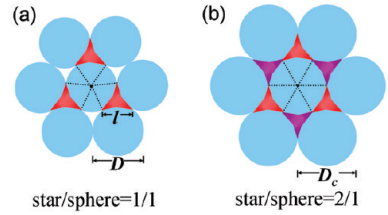

Scheme 4. Geometrical sketch of the size relationships between colloidal spheres and PbS nanostars. Here, D_c represents critical diameter of colloidal spheres for the formation of star−sphere binary colloidal crystals with a star/sphere ratio of 2.

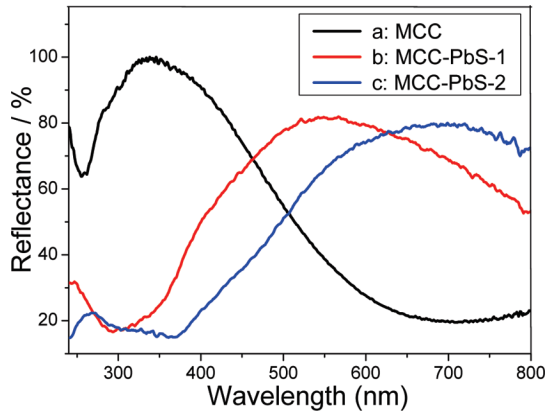

Figure 5. Reflection spectra of (a) 130 nm MCC template and (b,c) PbS nanostar arrays assembled on the template with different packing densities: (b) MCC-PbS-1 with a lower packing density as shown in Figure 3b−d, (c) MCC-PbS-2 with a higher packing density as shown in Figure 4.

PbS nanostars on the MCC template, the main reflection peak of the composite arrays significantly red-shifted, which could be simply attributed to the high refractive index for PbS.[62] Nevertheless, further calculation is needed to determine the stop band position of the composite arrays. These results indicate that the as-obtained MCC−PbS composite arrays could act as a photonic material with potential applications including thin film optical sensors.[63,64] It is also expected that the composite array might have interesting photonic properties in different incident directions due to its anisotropic star-shaped building blocks, which is currently under investigation in our lab.

The patterns of the PbS nanostar arrays can be readily adjusted by using MCCs with different sphere diameters as the template under otherwise identical conditions. For example, two MCC templates consisting of 340 nm poly(methyl methacrylate) (PMMA) spheres and 500 nm polystyrene (PSt) spheres were employed for vertical deposition of PbS nanostars. Figure 6a shows the ncp array of PbS stars assembled in a lower PbS dispersion concentration (~0.75 mM) by using 340 nm spheres in the MCC template. Since the sphere diameter was larger than D_c (~150 nm), one PbS nanostar tended to occupy each interstitial site in the ordered MCC template layer, leading to a star-to-sphere number ratio of approximately 2. However, it is noteworthy that the size matching between the triangle-shaped interstice of MCC and the star-shaped particle would decrease with increasing the diameter of the polymer spheres, resulting in a significant deviation from the perfect binary star-sphere colloidal crystals with a star/sphere ratio of 2. If the PbS dispersion concentration was increased to ~1.5 mM, nanonet-like PbS nanostar arrays with a hole size of ~260 nm were assembled on the MCC template (Figure 6b). In this case, PbS nanostars tended to fill the gaps among the template layer with local ordered structure, leading to the nanonet-like arrays with ordered, hexagonally packed circular holes that were inherited from the original MCC templates. For the 500 nm MCC template, each interstitial site of the template could trap three to five PbS nanostars in an ordered arrangement under a lower PbS dispersion concentration (~1 mM), resulting in another novel pattern for ncp PbS nanostar array, as demonstrated in Figure 6c. Similarly, if the PbS dispersion concentration was increased to ~2 mM, nanonet-like PbS nanostar arrays with a hole size of ~390 nm were assembled on the MCC template (Figure 6d).

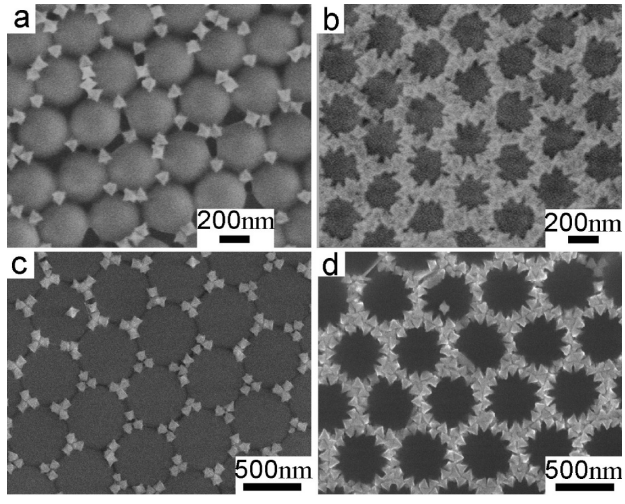

Figure 6. SEM images of patterned arrays of PbS nanostars assembled on the 340 nm (a,b) and 500 nm (c,d) MCC templates with a lower (a,c) and higher (b,d) packing densities by vertical deposition.

Patterned Arrays of PbS Nanostars Assisted by IMCC. As illustrated in Scheme 3B, [001]-oriented assemblies of PbS nanostars with a single [001]-oriented horn vertically standing on the template (designated as ncp array-2) can be obtained through IMCC template-directed vertical deposition. A silica IMCC film on a Si substrate was fabricated by replicating the prepared MCC of polymer spheres with silica, which was followed by extracting the polymer spheres with toluene. A typical SEM image of the as-replicated silica IMCC film templated by 130 nm P(St-MMA) spheres is shown in Figure 7a, which shows a honeycomb-like structure, inheriting the long-range hexagonal order from the initial MCC template. A closer view shown in Figure 7b reveals that there is a circular gap with a diameter of ~50 nm on the top of the IMCC template, which is significantly smaller than the diameter of the colloidal spheres, indicating that the height of the silica filling is considerably higher than the colloidal sphere equators. This IMCC consisting of relatively deep cavities with narrow necks can serve as a unique template for the orientation-specific assembly of PbS nanostars. Figure 7c shows a top view of the PbS ncp array assembled in proper PbS dispersion concentration (~1 mM) by using a 130 nm IMCC template. As can be seen, each nanostar is strictly oriented with a single

horn inserted into the circular gap of the IMCC template and the opposite horn stretched vertically upward. Figure 7d illustrates clearly that the orderly aligned nanostars reserved the hexagonal periodicity of the IMCC template.

It was found that the size of the circular gap on the top of the IMCC template, which was determined by the silica filling height, showed a remarkable effect on the formation of ncp PbS arrays with different orientations. For the situation shown in Figure 7a,b, the height of the silica filling is much higher than the colloidal sphere equators. For comparison, a thinner silica IMCC template was fabricated by infiltrating a silica sol with a lower concentration, which reveals a circular gap with a diameter of ~110 nm on top (Figure 8a). In this case, the silica filling height was much lower than that in Figure 7a,b, and the PbS nanostars tended to deposit on the template with three horns stably inserted into the interstitial site to form [111]-oriented assemblies after vertical deposition (Figure 8b). So the size matching between circular gaps on the top of the IMCC template and the stretched horns of PbS nanostars is essential for the formation of the ncp array of [001]-oriented PbS nanostars.

Moreover, other patterned arrays of PbS nanostars can be conveniently fabricated by using silica IMCC with larger size cavities as the template through vertical deposition. For example, when the size of initial polymer spheres of the MCC template was increased from 130 to 500 nm, silica IMCC with a cavity size of ~500 nm was obtained, and PbS nanostars tended to fill the hexagonally ordered cavities completely at a proper PbS dispersion concentration (~2 mM) after vertical deposition. The as-prepared PbS array exhibited ordered, hexagonally packed disk-like units that were inherited from the original IMCC template (Supporting Information, Figure S3a). It can be seen from a magnified image that about 20 nanostars were filled in each cavity with disordered structure to constitute the disk-like unit of the patterned array (Supporting Information, Figure S3b). However, further study is still needed to fully investigate the effect of such parameters (such as cavity size and pore opening) on the degree of uniformity in nanostar orientation, which is decidedly of interest. In this regard, the orientation of the stars both out of the IMCC surface plane and in the plane might be well-controlled if the silica filling height could be accurately adjusted combined with the use of colloidal spheres with varied sizes.

CONCLUSIONS

Controllable self-assembly of star-shaped PbS nanocrystals into both close-packed arrays and patterned arrays was demonstrated for the first time. First, large-area 3D and 2D hcp assemblies of PbS nanostars were obtained on clean Si substrate by drop coating and vertical deposition, respectively. Interestingly, by using

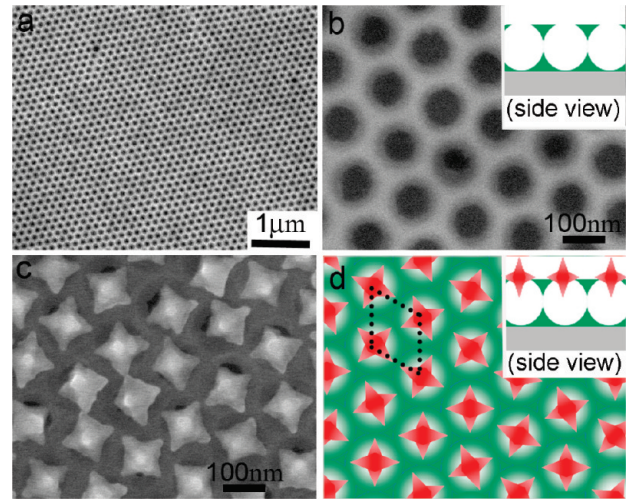

Figure 7. SEM images of (a,b) silica IMCC templated by 130 nm colloidal spheres and (c) ncp array of PbS nanostars assembled on the IMCC template by vertical deposition. (d) Schematic illustration of the 2D ncp array-2 of six-horn stars. Insets schematically illustrate the side view.

MCC and IMCC as the template, various ncp arrays of PbS nanostars with controllable patterns were fabricated through the vertical deposition method. With the 130 nm MCC template, an ncp array of [111]-oriented PbS nanostars with three horns stably standing on the template was prepared, leading to the formation of novel star−sphere binary colloidal crystals with a stoichiometric star/sphere ratio of 1. The photonic properties of the MCC−PbS composite arrays were also preliminarily investigated, which showed that the reflection peak still existed when PbS nanostars were assembled on the MCC template and it red-shifted with increasing the packing density of PbS nanostars. It was revealed that a proper concentration of initial PbS dispersions and the peculiar shape of six-horn stars were crucial for the exclusive formation of the ncp array of [111]-oriented PbS nanostars. With the 130 nm IMCC template, an ncp array of [001]-oriented PbS nanostars with a single horn stretched vertically upward was prepared, and the suited size of circular gaps on the surface plane of the IMCC template (*i.e.*, the proper silica filling height) was essential besides the peculiar six-horn

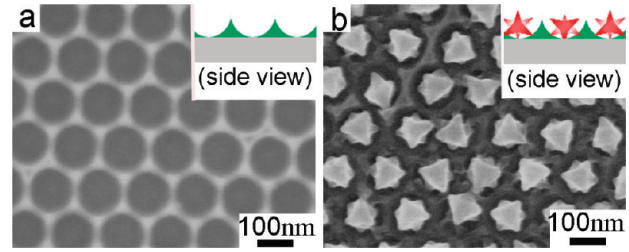

Figure 8. SEM images of (a) silica IMCC with a lower height templated by 130 nm colloidal spheres and (b) PbS nanostar array assembled on the IMCC template by vertical deposition. Insets schematically illustrate the side view.

star shape of PbS nanocrystals. Furthermore, some novel patterns for the PbS ncp array were readily fabricated using MCC/IMCC templates with larger periodic spacings. It is worth mentioning that, for the template-assisted assembly of PbS nanostars, almost all of the PbS ncp arrays inherited the long-range hexagonal order from the initial MCC template. The obtained PbS close-packed and patterned arrays may exhibit novel physical properties by virtue of the peculiar six-horn star shape of PbS nanocrystals as well as their well-defined locations and orientations and could find potential applications including photoelectronic and photonic nanodevices. The assembly strategy described here is a versatile approach and may open a new route for the controlled assembly of anisotropic nanostructured materials into large-scale ordered arrays with desirable patterns, which is essential for the success of bottom-up approaches toward future nanodevices with novel collective properties.

METHODS

Materials Synthesis. The star-shaped PbS nanocrystals were synthesized by the thermal decomposition of thioacetamide (TAA) in aqueous solutions of lead acetate in the presence of the cationic surfactant cetyltrimethylammonium bromide (CTAB) and the anionic surfactant sodium dodecyl sulfate (SDS), as described previously.[51] Monodisperse poly(styrene methyl methacrylate) (P(St-MMA)), poly(methyl methacrylate) (PMMA), and polystyrene (PSt) colloidal spheres were prepared according to the methods reported previously.[65,66]

MCC/IMCC Fabrication. The MCC template was fabricated on a Si substrate using a method recently developed at our lab.[35,36] For the preparation of the MCC template, 10 μL of water/ethanol dispersion containing monodisperse polymer colloidal spheres was dropped onto the top surface of a 1 × 1 cm piece of glass surrounded by water located at the midbottom of a Petri dish. The dispersion spread freely on the water surface until it covered nearly the whole surface area, resulting in a colorful MCC film up to ~16 cm^2 in area. Then the MCC film was picked up with a Si plate, and the patterned substrate covered with MCC was kept in vacuum prior to use. To generate the IMCC template on a Si substrate, the Si plate with MCC was infiltrated with silica sol.[35] After silification, the patterned substrate covered with IMCC was obtained by extracting the polymer MCC using toluene. The thickness of IMCC could be readily controlled by simply varying the concentrations of silica sol.

Nanocrystal Assembly. The as-prepared PbS nanocrystals were collected by centrifugation and redispersed in water, resulting in the formation of PbS nanocrystal dispersions with various concentrations. The 3D hcp assemblies of PbS nanostars were prepared using a simple drop coating method. Briefly, a drop (~30 μL) of the PbS dispersion with the concentration of ~30 mM was placed onto a clean Si substrate. The droplet was left uncovered and allowed to evaporate at room temperature. After evaporation, a ring made up of PbS nanoparticle assemblies was observed on the substrate. For the preparation of 2D hcp assemblies and differently patterned assemblies of PbS nanocrystals, the vertical deposition method was employed. The dispersion of PbS nanocrystals in water with proper concentration (1 mL) was added into a clean 2 mL cuvette, followed by vertically inserting a panel of clean Si substrate or patterned substrate covered with MCC/IMCC. The cuvette was kept undisturbed at room temperature over several days to deposit a uniform film of PbS assemblies on the substrate after the evaporation was complete.

Characterization. The samples were characterized by scanning electron microscopy (SEM, Hitachi FE-S4800, 2 or 5 kV), transmission electron microscopy (TEM, JEOL JEM-200CX, 160 kV), and optical microscopy (Nikon E600). Optical reflection spectra with normal incidence were recorded using a Hitachi U-4100 UV−vis−NIR spectrometer with a 5° specular reflectance accessory.

Acknowledgment. We gratefully acknowledge financial support from NSFC (Grants 20873002, 20673007, 20633010, and 50821061), MOST (Grant 2007CB936201), and SRFDP (Grant 20070001018).

Supporting Information Available: SEM and TEM images of an individual star-shaped PbS nanocrystal, optical photograph and micrograph of a coffee ring of PbS nanostar assemblies formed by drop coating, and SEM images of patterned array of PbS nanostars assembled on the 500 nm IMCC template. This material is available free of charge *via* the Internet at http://pubs.acs.org.

REFERENCES AND NOTES

1. Talapin, D. V.; Lee, J.-S.; Kovalenko, M. V.; Shevchenko, E. V. Prospects of Colloidal Nanocrystals for Electronic and Optoelectronic Applications. *Chem. Rev.* **2010**, *110*, 389–458.
2. Srivastava, S.; Kotov, N. A. Nanoparticle Assembly for 1D and 2D Ordered Structures. *Soft Matter* **2009**, *5*, 1146–1156.
3. Nie, Z. H.; Petukhova, A.; Kumacheva, E. Properties and Emerging Applications of Self-Assembled Structures Made from Inorganic Nanoparticles. *Nat. Nanotechnol.* **2010**, *5*, 15–25.
4. Kinge, S.; Crego-Calama, M.; Reinhoudt, D. N. Self-Assembling Nanoparticles at Surfaces and Interfaces. *ChemPhysChem* **2008**, *9*, 20–42.
5. Velev, O. D.; Gupta, S. Materials Fabricated by Micro- and Nanoparticle Assembly—The Challenging Path from Science to Engineering. *Adv. Mater.* **2009**, *21*, 1897–1905.
6. Jana, N. R. Shape Effect in Nanoparticle Self-Assembly. *Angew. Chem., Int. Ed.* **2004**, *43*, 1536–1540.
7. Jun, Y.; Choi, J.; Cheon, J. Shape Control of Semiconductor and Metal Oxide Nanocrystals through Nonhydrolytic Colloidal Routes. *Angew. Chem., Int. Ed.* **2006**, *45*, 3414–3439.
8. Xia, Y.; Xiong, Y.; Lim, B.; Skrabalak, S. E. Shape-Controlled Synthesis of Metal Nanocrystals: Simple Chemistry Meets Complex Physics. *Angew. Chem., Int. Ed.* **2009**, *48*, 60–103.
9. Sau, T. K.; Rogach, A. L. Nonspherical Noble Metal Nanoparticles: Colloid-Chemical Synthesis and Morphology Control. *Adv. Mater.* **2010**, *22*, 1781–1804.
10. Shevchenko, E. V.; Talapin, D. V.; Kotov, N. A.; O'Brien, S.; Murray, C. B. Structural Diversity in Binary Nanoparticle Superlattices. *Nature* **2006**, *439*, 55–59.
11. Talapin, D. V.; Shevchenko, E. V.; Bodnarchuk, M. I.; Ye, X.; Chen, J.; Murray, C. B. Quasicrystalline Order in Self-Assembled Binary Nanoparticle Superlattices. *Nature* **2009**, *461*, 964–967.
12. Glotzer, S. C.; Solomon, M. J. Anisotropy of Building Blocks and Their Assembly into Complex Structures. *Nat. Mater.* **2007**, *6*, 557–562.
13. Min, Y. J.; Akbulut, M.; Kristiansen, K.; Golan, Y.; Israelachvili, J. The Role of Interparticle and External Forces in Nanoparticle Assembly. *Nat. Mater.* **2008**, *7*, 527–538.
14. Sau, T. K.; Rogach, A. L.; Jackel, F.; Klar, T. A.; Feldmann, J. Properties and Applications of Colloidal Nonspherical Noble Metal Nanoparticles. *Adv. Mater.* **2010**, *22*, 1805–1825.
15. Ming, T.; Kou, X.; Chen, H.; Wang, T.; Tam, H.-L.; Cheah, K.-

W.; Chen, J.-Y.; Wang, J. Ordered Gold Nanostructure Assemblies Formed by Droplet Evaporation. *Angew. Chem., Int. Ed.* **2008**, *47*, 9685–9690.
16. Guerrero-Martinez, A.; Perez-Juste, J.; Carbo-Argibay, E.; Tardajos, G.; Liz-Marzan, L. M. Gemini Surfactant-Directed Self-Assembly of Monodisperse Gold Nanorods into Standing Superlattices. *Angew. Chem., Int. Ed.* **2009**, *48*, 9484–9488.
17. Baker, J. L.; Widmer-Cooper, A.; Toney, M. F.; Geissler, P. L.; Alivisatos, A. P. Device-Scale Perpendicular Alignment of Colloidal Nanorods. *Nano Lett.* **2010**, *10*, 195–201.
18. Baranov, D.; Fiore, A.; van Huis, M.; Giannini, C.; Falqui, A.; Lafont, U.; Zandbergen, H.; Zanella, M.; Cingolani, R.; Manna, L. Assembly of Colloidal Semiconductor Nanorods in Solution by Depletion Attraction. *Nano Lett.* **2010**, *10*, 743–749.
19. Ding, T.; Song, K.; Clays, K.; Tung, C.-H. Fabrication of 3D Photonic Crystals of Ellipsoids: Convective Self-Assembly in Magnetic Field. *Adv. Mater.* **2009**, *21*, 1936–1940.
20. Cao, Y. C. Synthesis of Square Gadolinium-Oxide Nanoplates. *J. Am. Chem. Soc.* **2004**, *126*, 7456–7457.
21. Zhang, Y.-W.; Sun, X.; Si, R.; You, L.-P.; Yan, C.-H. Single-Crystalline and Monodisperse LaF_3 Triangular Nanoplates from a Single-Source Precursor. *J. Am. Chem. Soc.* **2005**, *127*, 3260–3261.
22. Zhou, H.-P.; Zhang, C.; Yan, C.-H. Controllable Assembly of Diverse Rare-Earth Nanocrystals *via* the Langmuir−Blodgett Technique and the Underlying Size- and Symmetry-Dependent Assembly Kinetics. *Langmuir* **2009**, *25*, 12914–12925.
23. Tao, A. R.; Sinsermsuksakul, P.; Yang, P. Tunable Plasmonic Lattices of Silver Nanocrystals. *Nat. Nanotechnol.* **2007**, *2*, 435–440.
24. Tao, A. R.; Ceperley, D. P.; Sinsermsuksakul, P.; Neureuther, A. R.; Yang, P. Self-Organized Silver Nanoparticles for Three-Dimensional Plasmonic Crystals. *Nano Lett.* **2008**, *8*, 4033–4038.
25. Mokari, T.; Zhang, M.; Yang, P. Shape, Size, and Assembly Control of PbTe Nanocrystals. *J. Am. Chem. Soc.* **2007**, *129*, 9864–9865.
26. Goodman, M. D.; Zhao, L.; DeRocher, K. A.; Wang, J.; Mallapragada, S. K.; Lin, Z. Self-Assembly of CdTe Tetrapods into Network Monolayers at the Air/Water Interface. *ACS Nano* **2010**, *4*, 2043–2050.
27. Grzybowski, B. A.; Wilmer, C. E.; Kim, J.; Browne, K. P.; Bishop, K. J. M. Self-Assembly: From Crystals to Cells. *Soft Matter* **2009**, *5*, 1110–1128.
28. Galatsis, K.; Wang, K. L.; Ozkan, M.; Ozkan, C. S.; Huang, Y.; Chang, J. P.; Monbouquette, H. G.; Chen, Y.; Nealey, P.; Botros, Y. Patterning and Templating for Nanoelectronics. *Adv. Mater.* **2010**, *22*, 769–778.
29. Zhao, Y.; Thorkelsson, K.; Mastroianni, A. J.; Schilling, T.; Luther, J. M.; Rancatore, B. J.; Matsunaga, K.; Jinnai, H.; Wu, Y.; Poulsen, D.; Frechet, J. M. J.; Alivisatos, A. P.; Xu, T. Small-Molecule-Directed NP Assembly towards Stimuli-Responsive Nanocomposites. *Nat. Mater.* **2009**, *8*, 979–985.
30. Cheng, W.; Campolongo, M. J.; Cha, J. J.; Tan, S. J.; Umbach, C. C.; Muller, D. A.; Luo, D. Free-Standing Nanoparticle Superlattice Sheets Controlled by DNA. *Nat. Mater.* **2009**, *8*, 519–525.
31. Yin, Y.; Xia, Y. Self-Assembly of Monodispersed Spherical Colloids into Complex Aggregates with Well-Defined Sizes, Shapes, and Structures. *Adv. Mater.* **2001**, *13*, 267–271.
32. Yin, Y.; Lu, Y.; Gates, B.; Xia, Y. Template-Assisted Self-Assembly: A Practical Route to Complex Aggregates of Monodispersed Colloids with Well-Defined Sizes, Shapes, and Structures. *J. Am. Chem. Soc.* **2001**, *123*, 8718–8729.
33. Xia, Y.; Yin, Y.; Lu, Y.; McLellan, L. Template-Assisted Self-Assembly of Spherical Colloids into Complex and Controllable Structures. *Adv. Funct. Mater.* **2003**, *13*, 907–918.
34. Li, Y.; Cai, W.; Duan, G. Ordered Micro Nanostructured Arrays Based on the Monolayer Colloidal Crystals. *Chem. Mater.* **2008**, *20*, 615–624.
35. Li, C.; Hong, G.; Wang, P.; Yu, D.; Qi, L. Wet Chemical Approaches to Patterned Arrays of Well-Aligned ZnO Nanopillars Assisted by Monolayer Colloidal Crystals. *Chem. Mater.* **2009**, *21*, 891–897.
36. Li, C.; Hong, G.; Qi, L. Nanosphere Lithography at the Gas/Liquid Interface: A General Approach towards Free-Standing High-Quality Nanonets. *Chem. Mater.* **2010**, *22*, 476–481.
37. Chen, J.; Liao, W.-S.; Chen, X.; Yang, T.; Wark, S. E.; Son, D. H.; Batteas, J. D.; Cremer, P. S. Evaporation-Induced Assembly of Quantum Dots into Nanorings. *ACS Nano* **2009**, *3*, 173–180.
38. Rycenga, M.; Camargo, P. H. C.; Xia, Y. Template-Assisted Self-Assembly: A Versatile Approach to Complex Micro- and Nanostructures. *Soft Matter* **2009**, *5*, 1129–1136.
39. Zhang, Q.; Gupta, S.; Emrick, T.; Russell, T. P. Surface-Functionalized CdSe Nanorods for Assembly in Diblock Copolymer Templates. *J. Am. Chem. Soc.* **2006**, *128*, 3898–3899.
40. Deshmukh, R. D.; Liu, Y.; Composto, R. J. Two-Dimensional Confinement of Nanorods in Block Copolymer Domains. *Nano Lett.* **2007**, *7*, 3662–3668.
41. Ploshnik, E.; Salant, A.; Banin, U.; Shenhar, R. Hierarchical Surface Patterns of Nanorods Obtained by Co-assembly with Block Copolymers in Ultrathin Films. *Adv. Mater.* **2010**, *22*, 2774–2779.
42. Hong, S. W.; Jeong, W.; Ko, H.; Kessler, M. R.; Tsukruk, V. V.; Lin, Z. Directed Self-Assembly of Gradient Concentric Carbon Nanotube Rings. *Adv. Funct. Mater.* **2008**, *18*, 2114–2122.
43. Khanal, B. P.; Zubarev, E. R. Rings of Nanorods. *Angew. Chem., Int. Ed.* **2007**, *46*, 2195–2198.
44. Cui, Y.; Bjork, M. T.; Liddle, J. A.; Sonnichsen, C.; Boussert, B.; Alivisatos, A. P. Integration of Colloidal Nanocrystals into Lithographically Patterned Devices. *Nano Lett.* **2004**, *4*, 1093–1098.
45. Konstantatos1, G.; Howard, I.; Fischer, A.; Hoogland, S.; Clifford, J.; Klem, E.; Levina, L.; Sargent, E. H. Ultrasensitive Solution-Cast Quantum Dot Photodetectors. *Nature* **2006**, *442*, 180–183.
46. Rogach, A. L.; Eychmuller, A.; Hickey, S. G.; Kershaw, S. V. Infrared-Emitting Colloidal Nanocrystals: Synthesis, Assembly, Spectroscopy, and Application. *Small* **2007**, *3*, 536–557.
47. Patla, I.; Acharya, S.; Zeiri, L.; Israelachvili, J.; Efrima, S.; Golan, Y. Synthesis, Two-Dimensional Assembly, and Surface Pressure-Induced Coalescence of Ultranarrow PbS Nanowires. *Nano Lett.* **2007**, *7*, 1459–1462.
48. Ghadimi, A.; Cademartiri, L.; Kamp, U.; Ozin, G. A. Plasma within Templates: Molding Flexible Nanocrystal Solids into Multifunctional Architectures. *Nano Lett.* **2007**, *7*, 3864–3868.
49. Wang, N.; Cao, X.; Guo, L.; Yang, S.; Wu, Z. Facile Synthesis of PbS Truncated Octahedron Crystals with High Symmetry and Their Large-Scale Assembly into Regular Patterns by a Simple Solution Route. *ACS Nano* **2008**, *2*, 184–190.
50. Rupich, S. M.; Shevchenko, E. V.; Bodnarchuk, M. I.; Lee, B.; Talapin, D. V. Size-Dependent Multiple Twinning in Nanocrystal Superlattices. *J. Am. Chem. Soc.* **2010**, *132*, 289–296.
51. Zhao, N.; Qi, L. Low-Temperature Synthesis of Star-Shaped PbS Nanocrystals in Aqueous Solutions of Mixed Cationic-Anionic Surfactants. *Adv. Mater.* **2006**, *18*, 359–362.
52. Deegan, R. D.; Bakajin, O.; Dupont, T. F.; Huber, G.; Nagel, S. R.; Witten, T. A. Capillary Flow as the Cause of Ring Stains from Dried Liquid Drops. *Nature* **1997**, *389*, 827–829.
53. Deegan, R. D. Pattern Formation in Drying Drops. *Phys. Rev. E* **2000**, *61*, 475–485.

54. Shen, X.; Ho, C.-M.; Wong, T.-S. Minimal Size of Coffee Ring Structure. *J. Phys. Chem. B* **2010**, *114*, 5269–5274.
55. Jiang, P.; Bertone, J. F.; Hwang, K. S.; Colvin, V. L. Single-Crystal Colloidal Multilayers of Controlled Thickness. *Chem. Mater.* **1999**, *11*, 2132–2140.
56. Norris, D. J.; Arlinghaus, E. G.; Meng, L.; Heiny, R.; Scriven, L. E. Opaline Photonic Crystals: How Does Self-Assembly Work? *Adv. Mater.* **2004**, *16*, 1393–1399.
57. Vlasov, Y. A.; Bo, X.-Z.; Sturm, J. C.; Norris, D. J. On-Chip Natural Assembly of Silicon Photonic Bandgap Crystals. *Nature* **2001**, *414*, 289–293.
58. Marlow, F.; Muldarisnur; Sharifi, P.; Brinkmann, R.; Mendive, C. Opals: Status and Prospects. *Angew. Chem., Int. Ed.* **2009**, *48*, 6212–6233.
59. Velikov, K. P.; Christova, C. G.; Dullens, R. P. A.; van Blaaderen, A. Layer-by-Layer Growth of Binary Colloidal Crystals. *Science* **2002**, *296*, 106–109.
60. Jiang, P.; Prasad, T.; McFarland, M. J.; Colvin, V. L. Two-Dimensional Nonclose-Packed Colloidal Crystals Formed by Spincoating. *Appl. Phys. Lett.* **2006**, *89*, 011908.
61. Venkatesh, S.; Jiang, P. Generalized Fabrication of Two-Dimensional Non-Close-Packed Colloidal Crystals. *Langmuir* **2007**, *23*, 8231–8235.
62. Lv, C.; Guan, C.; Liu, Y.; Cheng, Y.; Yang, B. PbS/Polymer Nanocomposite Optical Materials with High Refractive Index. *Chem. Mater.* **2005**, *17*, 2448–2454.
63. Yates, H. M.; Pemble, M. E.; Palacios-Lidon, E.; Garcia-Santamaria, F.; Rodriguez, I.; Meseguer, F.; Lopez, C. Modification of the Natural Bandgap of Synthetic Opals *via* Infilling with Crystalline InP. *Adv. Funct. Mater.* **2005**, *15*, 411–417.
64. Duan, G.; Cai, W.; Luo, Y.; Sun, F. A Hierarchically Structured $Ni(OH)_2$ Monolayer Hollow-Sphere Array and Its Tunable Optical Properties over a Large Region. *Adv. Funct. Mater.* **2007**, *17*, 644–650.
65. Schroden, R. C.; Al-Daous, M.; Sokolov, S.; Melde, B. J.; Lytle, J. C.; Stein, A.; Carbajo, M. C.; Fernandez, J. T.; Rodriguez, E. E. Hybrid Macroporous Materials for Heavy Metal Ion Adsorption. *J. Mater. Chem.* **2002**, *12*, 3261–3267.
66. Holland, B. T.; Blanford, C. F.; Do, T.; Stein, A. Synthesis of Highly Ordered, Three-Dimensional, Macroporous Structures of Amorphous or Crystalline Inorganic Oxides, Phosphates, and Hybrid Composites. *Chem. Mater.* **1999**, *11*, 795–805.